

# Scalar transfer across the air-water turbulent interface

Z. F. XU<sup>1</sup>, B. C. KHOO<sup>1</sup>, K. Carpenter<sup>2</sup>

<sup>1</sup>Department of mechanical Engineering, National University of Singapore,  
Kent Ridge, Singapore 119260

<sup>2</sup>Institute of Chemical and Engineering Sciences, 1 Pesek Rd, Singapore, 627833

## Abstract

Mass transfer across the gas-water interface is important in many fields, but the present understanding of the scalar transport as mediated by the complex near-surface turbulence is still far from complete. In this work, an innovative PIV based measurement method was employed to investigate the near surface turbulence. Turbulence measurement with respect to the fluctuating interface was performed and the gradient of the vertical fluctuating velocity (Hanratty's  $\beta$ ) deemed as a critical controlling parameter was quantified. Several distinctly different but typical flow conditions were investigated and the associated mass transfer coefficient was measured. Based on these experimental works, an empirical relation, very similar to the earlier Law and Khoo's <sup>[1]</sup>, relating the mass transport across the turbulent interface to the turbulence parameter  $\beta$  was determined in the midst of vastly different flow conditions where turbulence is induced simultaneously from above and beneath the gas-water interface..

**Topical heading:** Fluid mechanics and transport phenomena

**Key words:** mass transfer, gas-water interface, Hanratty's  $\beta$ , linear region, PIV

## Introduction

Scalar transport across the turbulent gas-water interface has enormous importance in various natural and man-made industrial processes. Because of its wide application, a general model capable of predicting the scalar (heat or mass) transfer coefficient across the gas-water interface is highly desirable and remains the objective of many researchers. The interfacial mass transfer is, by its very nature, highly complex: the gas and the water may be in a state of turbulent motion, and the interface

is highly irregular, and possibly accompanied by waves with and without wave breaking and the associated entrainment and formation of bubbles.

For sparingly soluble gases, the diffusivity in the gaseous phase is usually much larger than in water. Hence the gas-side dynamics are less critical, and the transport is determined predominantly by the water-side hydrodynamics. Mass transfer of gases through the gas-water interface is affected by many factors, such as the difference of concentration between the phases, temperature, flow conditions and even more so the conditions or state of turbulence motion right at the interface where the expected concentration boundary layer is embedded. Molder et al <sup>[2]</sup>, Vasconcelos et al <sup>[3]</sup> and McKenna & McGillis <sup>[4]</sup> did further analysis on the effect of surfactants and insoluble compounds presence on the interface. It is surmised that the surfactants/contaminations can physically interfere with the transfer process or dampen and reduce the turbulent motion in the vicinity of the interface.

In the absence of the above-mentioned surface-seeking contaminations and surfactants, the state of turbulent motion in the vicinity of the interface where the concentration boundary is embedded is deemed to be the dominant factor affecting the transport rate across the interface. To correlate the mass transfer coefficient with suitable hydrodynamics parameters reflecting the turbulence conditions, many theories have been proposed to describe the mechanism governing the gas-water mass transfer. Theofanous <sup>[5]</sup>, in a review of various conceptual models, identified these different models into two major classes: eddy diffusivity model and eddy structure model. In the eddy diffusivity model, a relation between the mass transfer coefficient  $K_L$ , the diffusion coefficient  $D$ , and the thickness of the diffusion film  $\delta$  is proposed as:

$$K_L = \frac{D}{\delta}. \quad (1)$$

As such, the thickness of the diffusion film  $\delta$  is selected to characterize the hydrodynamics near the interface. The other class is the eddy structure model. It is also known as ‘surface renewal’ model. The model is expressed in the form as:

$$K_L = \sqrt{\frac{D}{\tau}}. \quad (2)$$

The averaged surface renewal time ( $\tau$ ) is thought to govern the mass transfer across the water interface. The difficulty with these conceptual models is that somehow the selected parameters ( $\delta$  or  $\tau$ ) must still be reasonably easy to characterize and make related to the near interface turbulence controlling the mass transfer. As Tamburrino & Gulliver <sup>[6]</sup> mentioned, the measurements of ‘surface renewal eddies’ are difficult to correlate with the mass transfer coefficient because the investigators themselves have to define what constitutes a surface renewal eddy.

Until now, there has been no broad consensus as to a general and yet sufficiently robust model which is capable of predicting the transfer coefficient under different flow conditions. Most models are based on parameters that are directly dependent on the particular means of turbulence generation and/or experimental set-ups and geometries. Such models may not be applicable under other turbulence conditions. Fundamentally, the exchange of gases across the gas-water interface occurs across a thin boundary layer at the gas-water interface. The details of the boundary layer are determined by the hydrodynamics near the surface. A robust model should be based primarily on the hydrodynamic parameters obtained directly from the turbulence structure in the very vicinity of the interface.

In a review of various works, Hanratty <sup>[7]</sup> highlighted the development of a model that relates the mass transfer coefficient directly to the hydrodynamics near the interface without resorting directly to the above-mentioned conceptual models. Since the concentration boundary layer is very thin, the derivative in the normal direction ( $z$ -) is much larger than in the other directions. Therefore, using a coordinate system embedded on the interface, the boundary-layer equation for concentration ( $C$ ) in a turbulent flow field near a free surface can be simplified as:

$$\frac{\partial C}{\partial t} + w \frac{\partial C}{\partial z} = D \frac{\partial^2 C}{\partial z^2}. \quad (3)$$

McCready et al <sup>[8]</sup> conducted a series expansion and order-of-magnitude analysis near the interface and deduced the following relation for the vertical velocity

$$w = \beta z . \quad (4)$$

That is, at the vicinity of the interface,  $w$  varies linearly with  $z$  with a gradient of  $\beta$ . From Equations (3) and (4), the importance of  $\beta$  is apparent to mass transfer across the gas-water interface.

The interest in  $\beta$  as the crucial parameter governing the interface mass transfer provided the motivation for the development of a technique that can simultaneously measure the undulating interface and the flow field just beneath it. PIV-based technique provides an advantage of non-interference of the flow field and allows the measurements of the whole flow field at that same time to be carried out. Hassan et al [9], Peirson [10] and Law et al [11] and several other researchers have proposed some techniques based on PIV technique with the intention of measuring the interface fluctuation as well as the velocity just beneath it. Based on the measurement technique of Law et al [11], Law and Khoo [1] carried out a series of experimental works with two vastly different flow conditions and found that the selected near surface turbulence parameter ( $\beta$ ) provides a reasonable model for interfacial mass transfer. Their relation is expressed as:

$$K_L^+ Sc^{0.5} = 0.22 \beta_{rms}^{+0.5} . \quad (5)$$

This is perhaps the first time a correlation was presented to account for two very different means of turbulence generations: one from above in the gaseous phase and the other from beneath the interface in the water.

It is noted that these two different turbulence generation means were carried out separately: either from above or below, but not simultaneously. The validity and accuracy of the model is also not tested more extensively. In this work, it is our intent to improve on the measurement technique of Law and Khoo [1], and conduct a series of experiments with more varied flow conditions. In particular, the critical parameter  $\beta$  was measured for several representative flow conditions encountered in environment: turbulence generated from above (in the gaseous phase) as in wind-induced flow, turbulence generated simultaneously from above and below in the same direction, and simultaneously generated in the opposite direction. In the midst of

such measurements, the mass transfer experiment was carried out with the aim of providing a relationship between the mass transfer coefficient and the selected hydrodynamics parameter  $\beta$  for comparison with Law and Khoo <sup>[1]</sup>. In this work, oxygen is intentionally introduced and employed as the tracer gas instead of carbon dioxide as in Law & Khoo <sup>[1]</sup>, and a more general correlation is anticipated.

## Experimental approach

### Experimental set-ups

The experiment was carried out in a circular wind wave channel tank with two water jet streams directed in the tangential streamwise direction at the bottom. Figure 1 shows the schematic diagram of the circular water tank.

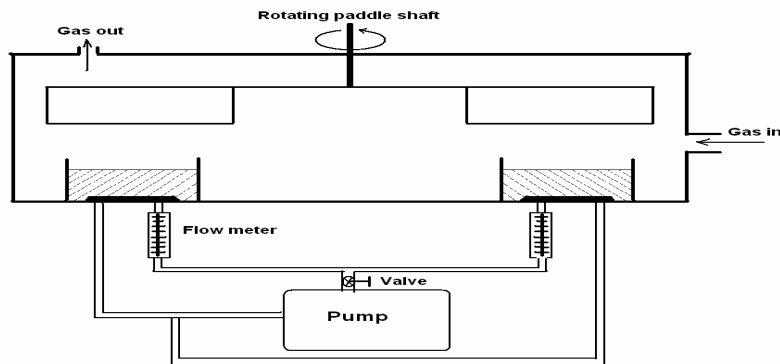


Figure 1: Schematic diagram of the circular water tank (not to scale)

It consisted of an annular water channel with 10-cm depth, 10-cm width with 40-cm ID and enclosed in a 75-cm diameter external cylindrical tank. The entire setup was made of transparent Perspex material, so as to facilitate flow visualization and measurement. The wind was generated by means of a rotor with four Perspex paddles (20cm width) arranged at right angles above the annular channel. The distance between the paddles and the water surface can be adjusted, and the rotating speed and rotating direction of the paddles was controlled by a rotor. The two water jet streams through four 3mm diameter nozzles (placed diametrically opposite) beneath the interface can generate a clockwise direction stream-wise flow directed along the bottom of the circular tank via the inlets and outlets connected to a water pump. The

speed of the water jet generated can be varied using a ball valve and the volumetric flow rate was measured with a flow meter. So by using these two independent means of turbulence generation from above and beneath the gas-water interface, we can get a variety of flow conditions imposed on the water surface and its vicinity. In this work, several representative kinds of flow conditions were chosen. These were generated via solely wind shear from above, and the simultaneous generation via wind shear from above and water jet from beneath in the same and opposite directions. These representations of turbulence generation are deemed more general and perhaps all encompassing. They can be considered as a reasonable simplification of most real life complex flow conditions.

In the experiments, fresh tap water was filled to a depth of 7.5 cm in the channel, and the paddles were located at about 7.5cm above the water surface. The flow rate through the water pump was adjusted with the combination of a ball valve and a flow meter. With a given flow rate from beneath, the turbulence intensity near the interface is still a function of the variable imposed wind speed. Table 1 summaries the groups of different flow conditions studied.

Table 1: Summary of the PIV experimental conditions

<b>Flow conditions</b>	<b>Flow rate (ml/s)</b>	<b>Direction</b>	<b>Nominal wind speed (m/s)</b>
Case 1	0		3, 3.5, 4, 4.5, 5, 5.5, 6, 6.5, 7
Case 2	6.3	Opposite	3, 3.5, 4, 4.5, 5, 5.5, 6, 6.5, 7
Case 3	6.3	Same	3, 3.5, 4, 4.5, 5, 5.5, 6, 6.5, 7
Case 4	3.2	Opposite	3.5, 4.5, 6, 6.5
Case 5	3.2	Same	3.5, 4.5, 6, 6.5
Case 6	10.5	Opposite	3.5, 4.5, 6, 6.5
Case 7	10.5	Same	3, 3.5, 4.5, 6, 6.5

For purpose of reference, the notional gas flow speed above the water surface is assumed to be the same as paddle speed which is taken directly above the center of the 10cm width water channel. This method of referencing follows that of Law et al [11], where

$$V_{wind} \approx R\omega. \quad (6)$$

Here  $\omega$  is the rotation speed of the rotor driving the paddles, and R is the distance from the center of the rotation shaft to the center of the water channel. The rotation speed of the rotor was measured using a tachometer. The paddle speed above the center of the water channel is taken as the parameter denoting the quality of turbulence generated at the water surface of the wind wave channel. Since the major or practically all of the resistance to the mass transfer in this experiment (low solubility gas is used) resides in the water side, accurate measurement of wind velocity profile in the vicinity of the interface is deemed unnecessary, and will not aid further in the quantification of the critical parameter influencing the interfacial mass transfer.

The range of nominal wind speeds carried out in this study is 3.00m/s to 7.00m/s. The upper limit wind speed is chosen such that the turbulence intensity generated is well below the limit where wave breaking occurs.

For these experiments, the circular wind wave channel is sealed by a gas tight lid. The tracer gas is input through the opening at the side of the tank, and residual gas is exhausted out of the system through the outlet opening located at the top.

### **Technique for measuring near surface turbulence**

The existence of a meniscus at the point of contact between the water and channel wall can cause some difficulties/uncertainties in visualizing the flow field at the vicinity of the interface. In the early PIV-based experiments (such as the works of Jahne & Wierzimok [12], Hassan et al [9]), the difficulties lie in determining the interface position accurately without affecting the near-surface flow conditions. Another class of method was based on the optic property of laser light, of which

representative works include Lorencez et al <sup>[13]</sup>, Baumann et al <sup>[14]</sup>, and Lin & Perlin <sup>[15]</sup>. This method, though capable of determining the interface position without affecting the near-surface flow conditions, did not allow or facilitate the simultaneous measurement of the flow field above and beneath the gas-water interface.

To avoid the effect of the meniscus, Munsterer & Jahne <sup>[16]</sup> suggested observing the interface and the flow field beneath it from a position slightly below the water surface. Peirson <sup>[10]</sup> used a camera to observe and determine the interface wave motion from above. It produced an unobstructed and good visualization of the interface. Inspired by these two mentioned works, Law et al <sup>[11]</sup> implemented two pairs of viewing mirrors to reflect the two different views onto a single plane.

In the present work, with the availability of two independent camera systems, further improvements can be made for a more accurate quantification of the interface position and improvement of the spatial resolution of the flow field close to the interface.

Figure 2 shows the schematic diagram for arrangement of the two titled cameras (Pixelfly, HiRes model). Camera 1 and camera 2 were adjusted separately and titled at a small angle of about  $7.5^\circ$  to the horizontal. These small angles, obtained after numerous trials, ensure unobstructed and clear visualization of the flow field for all of the imposed flow conditions, while keeping the magnification difference between the top and bottom (known as distortion) not exceeding 5%. To visualize the water surface as a continuous edge, fluorescent dye was introduced to illuminate the visualization plane. It is similar to the work of Law et al <sup>[11]</sup>.

The typical images captured simultaneously from camera 1 and camera 2 are also shown in Figure 2. With the introduction of fluorescent dye, the water side glows with certain luminance intensity, different from those of the particles. The interface is located at the edge of the contrast between the fluid and the gas. The advantage of using fluorescent dye to visualize the interface is that regardless of the interface fluctuation, the interface will always be visualized as a continuous edge of luminance contrast. The dye also produces contrasting luminance intensity from the particle seedings to allow the employment of PIV technique.

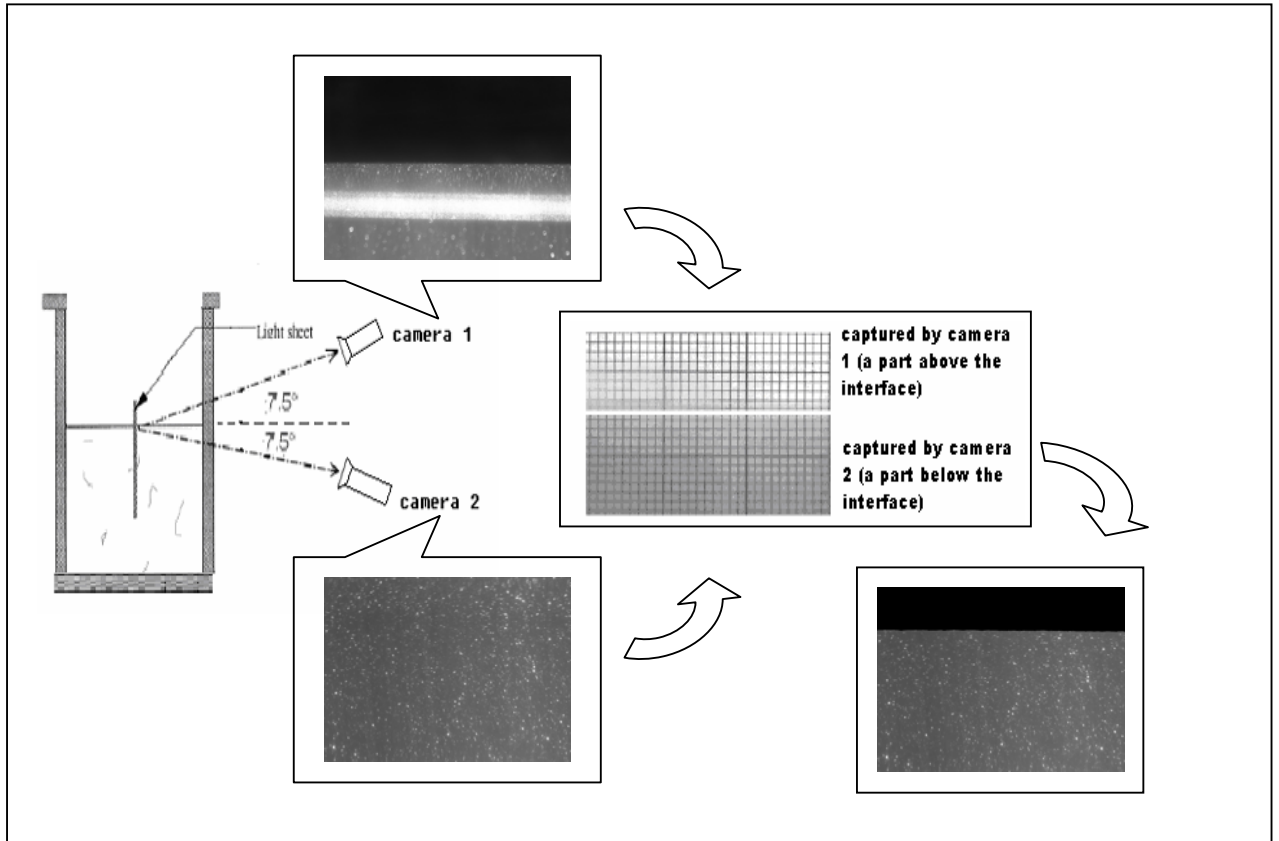


Figure 2: Schematic diagram of the observing angles and interface detection

Before the start of an experiment, a careful scaling calibration step is needed to correlate the images captured by camera 1 and camera 2. A referenced scale is set to ‘puncture’ the water surface at the plane of observation (coincide with the laser sheet plane). Images are captured by each of cameras and compared pixel by pixel. After obtaining the interface location from camera 1, a program is written to "transform" the interface location to the bottom view (camera 2) using the bottom view local scaling. The program is used to scale and correlate the images so that both the horizontal and vertical alignments are achieved. Some parts of the referenced scale images captured by the two cameras and the “transforming process” from camera 1 to camera 2 are also shown in Figure 2.

The conventional edge detection technique is based on finding the “maximum gradient” point. Since the particles (~20 $\mu\text{m}$  PSP) are brighter than water, edge detection working directly on the gray images of the gas-water interface (captured from camera 1) will detect the edge of particles and the interface simultaneously (see

Figure 3). To filter out the particles points seeded in the water side, an optimal threshold value of intensity is chosen to do binary operation. Taking account of the possible uneven distribution of light intensity along the interface, the interface region is divided into a subset of discretized surface regions and the binary operation is performed in each small part. The threshold level is determined by analyzing the histogram of the corresponding small part. A matlab program is written to perform all of these operations based on the technique described by Rider and Calvard <sup>[17]</sup>. After the binary operation, edge detection can then be used to determine the interface location. Figure 4 shows the interface profile detected by this method. It is shown to be accurate via comparison with the original image, and the uncertainty is controlled within  $\pm 1$ pixel. Figures 3 and 4 just show the region near the interface.

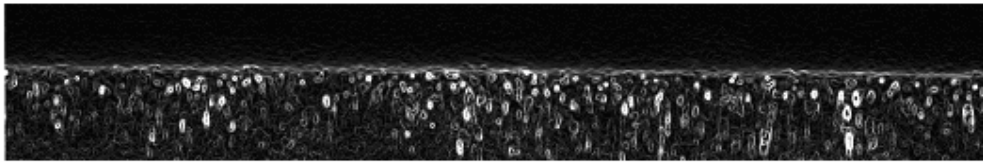


Figure 3: edge detection worked on the near surface region (gray image)



Figure 4: edge detection worked on the near surface region (binary image)

### **Technique for measuring the interfacial mass transfer coefficient**

In this work, mass transfer coefficient is determined by measuring the dissolved oxygen evasion rate and absorption rate. Gas exchange coefficients are determined by a disturbed equilibrium method. The water concentration of the dissolved oxygen to be measured is perturbed from equilibrium prior to an experiment and the gas transfer coefficient is computed by measuring the rate of return to equilibrium. The time rate of change in the tank of water is given by:

$$\frac{dC}{dt} = K_L A(C_s - C)/V_w \quad (8)$$

where  $V_w$  is the volume of water in the test system,  $A$  is the nominal area of the interface without waves,  $C$  is the bulk concentration of dissolved oxygen in water,  $C_s$  is the saturation concentration of oxygen at the interface and  $K_L$  is the bulk liquid-side mass transfer coefficient. The solution to Equation (8) is as follows:

$$K_L = \left( \frac{V_w}{At_f} \right) \ln \frac{(C_s - C_i)}{(C_s - C_f)}, \quad (9)$$

where  $C_i$  is the initial concentration of gas in the bulk water, and  $C_f$  is the final concentration after time  $t_f$ .

The mass transfer coefficient measurements were carried out separately from the turbulence measurements, and it is noted that precaution were taken to clean the interface well before each experiment just as discussed at length in Law and Khoo<sup>[1]</sup> and not repeated here. As the tracer gas is stored at a temperature cooler than the bulk water in the test section, it needs to be preheated to the same temperature before being introduced into the setup. This is done by passing the gas through a heat exchanger, immersed in a large water bath. The water temperature in the test section is monitored with a thermometer to make sure that the variation is below  $\pm 0.5$  °C. In the test section, the tracer gas is introduced just above the interface and with special care taken so as not to induce any interface disturbance. Before each experiment, the tracer gas is introduced for at least 20 minutes (for evasion experiments) or 10 minutes (for absorption experiments) to ensure a uniform initial condition. The most important aim is to prevent any build up of non-condensable gases (notably air) residing close to the interface.

For the gas evasion experiments,  $\text{CO}_2$  was used to continually flush the tank headspace to yield a known zero oxygen surface concentration, i.e.  $C_s(t) \approx 0 \text{ mg/l}$ . For gas absorption experiments, pure  $\text{O}_2$  was introduced such that the total gaseous volume above the interface was considered to be saturated. Under such condition,  $C_s$  is maintained at the water surface at water temperature; this value obtained from the manual supplied by the sensor manufacturer (in agreement with published measurements).

By measuring  $C_i$  and  $C_f$ , the water side mass transfer coefficient  $K_L$  can be determined. In this work, bulk water side dissolved oxygen concentration was measured using a commercial fiber optic oxygen sensor (INSTECH, model 210) with an accuracy of 1%. The sensor uses two standards of known oxygen concentration and a linear algorithm for calibration. In this work, the two known oxygen concentration standards are zero concentration standard and atmospheric saturated concentration standard. The zero standards are obtained by adding sodium sulfite to DI (Deionization) water. To prepare the atmospheric saturated standards, starting with DI water from a bottle held at ambient temperature for a long time, and transferring it from cup to cup with ample turbulence at least 20 times. This procedure followed the instruction of DQM standard operation procedure (Katzenlson <sup>[18]</sup>). Because of the theory of operation, the sensor will be most sensitive to low levels of oxygen and deviations from the linear relation occur primarily at higher oxygen concentration levels. The working range for oxygen evasion experiment was within the calibration range, while the absorption experiment was conducted in the extrapolated range of calibration. A shorter time interval was therefore adopted to take out the final water samples in the gas absorption experiment. This helps to ensure that the working range in the absorption experiment is not far away from the linear calibration range, although it maybe mentioned that the gas absorption experiment is still less accurate than the gas evasion experiment. Nevertheless these two means were employed as a self-consistent check and to demonstrate that essentially the correlation relationship obtained is independent of the direction of scalar transport.

Concentrations of  $C_i$  and  $C_f$  were obtained as the average values of at least 5 samples with a variation below 2%. Taking into account the measurement uncertainty introduced by the instrument calibration, the overall measurement uncertainty for gas evasion experiment is estimated to be below 5%. On the other hand, the measurement uncertainty for the gas absorption experiment is estimated to be about 10% or higher and attributed to the limitation posed by the oxygen probe.

## Data analysis and results

### Near surface vertical velocity gradient

Figure 5 shows the typical variation of the vertical fluctuating velocity with respect to the interface (for Case 3 with nominal wind speed=5m/s). It can be seen that the vertical fluctuating velocity measured with respect to the interface increases with the depth. This quantity tends towards zero as the interface is approached.

It can be seen from Figure 5 that a linear region appears to exist near the interface. This is in agreement with the analysis of McCready et al [8] and confirmed in the experiments of Law & Khoo [1]. A linear fit through the origin was performed on the data points located at the immediate vicinity of the interface to provide a  $R^2$  coefficient (coefficient of determination) still greater than 0.85 for all experiments.

The most important parameter  $\beta_{\text{rms}}$  is defined as the gradient of the  $V_{\text{r-rms}}$  profile near the interface, which can be deduced from Equations (3) and (4) to relate to the mass transfer across the turbulent gas-water interface.

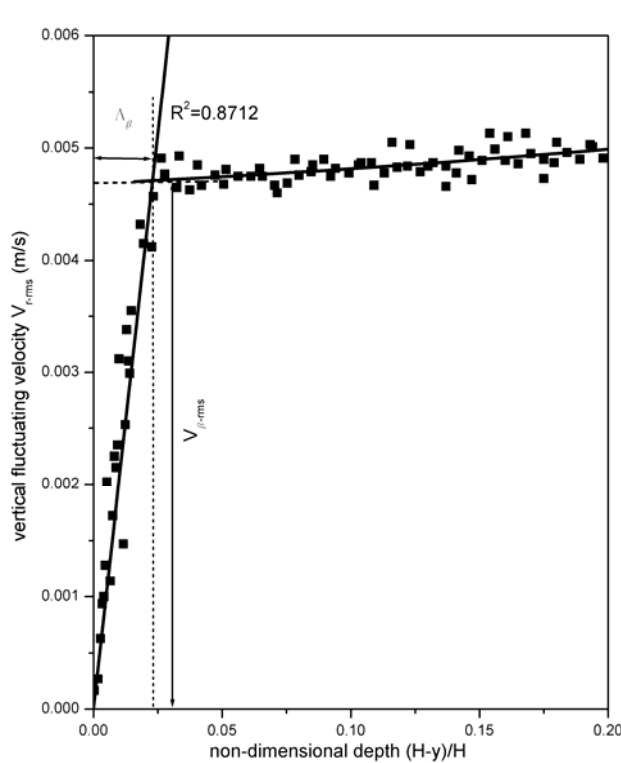


Figure 5: Variation of  $V_{\text{r-rms}}$  with non-dimensional depth

Figure 6 gives out the variation of  $\beta_{rms}$  with the nominal wind speeds for the all of the flow conditions studied. The results of Law & Khoo [1] for only wind induced flow conditions are also included. It can be seen that this selected parameter generally increased with the wind speed. It clearly indicates that the near surface turbulence intensity expressed in terms of  $\beta_{rms}$  in the linear region is dependent on the imposed wind speed from above and the water flow velocity from beneath. On the comparison of the different  $\beta_{rms}$  values under the same water flow rate, it can be seen that turbulence generated in co-current flow (i.e. the wind above and water below the interface are imposed in the same direction) is deemed to have the largest turbulence intensity in the vicinity of the interface region, while turbulence generated in countercurrent have the smallest turbulence intensity in that region. Under the lower water flow rate conditions (3.2ml/s and 6.3ml/s), Figure 6 indicates that the near surface turbulence is primarily determined by the wind speed induced from above. Lastly, it may be mentioned regarding the comparison of the present results to Law & Khoo [1] for the wind only, the deviations occur primarily in the low wind speed range, which are usually associated with lower flow velocities and larger measurement errors or uncertainties; the differences are limited to about 20%.

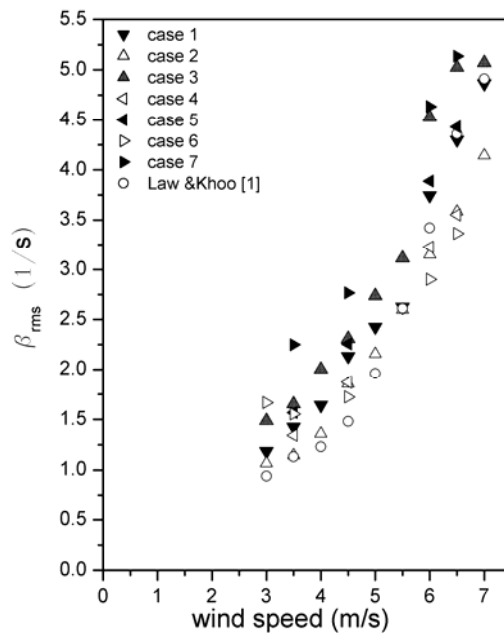


Figure 6: Variation of  $\beta_{rms}$  with nominal wind speed for Cases 1-7

## Mass transfer coefficient

Figure 7 gives out the mass transfer coefficient in the studied flow conditions. From this figure, it can be seen that the mass transfer coefficient generally increases with the wind speed. This again demonstrates the general trend between turbulence intensity with mass transfer coefficient. The mass transfer coefficient in Figure 7a shows a fairly linear behavior passing through the origin for the case where only wind speed is imposed. A closer scrutiny reveals that for the cases of same direction (Fig. 7b),  $K_L$  assumes a value perceptibly higher than the linear profile as obtained in Fig. 7a. On the other hand,  $K_L$  for the cases of opposite direction (Fig. 7c) takes on quantities clearly below the linear region depicted in Fig. 7a. This observation is not too surprising as deduced from Figure 6 if one presupposed that the mass transfer is directly proportional to  $\beta_{rms}$ . A careful examination of Figure 7a, 7b and 7c suggests that on comparing to the gas evasion results, the mass transfer coefficient obtained via the gas absorption experiment seems to assume a larger quantity and the difference tends to increase as the wind speed increases. Overall, the  $\beta_{rms}$  data of Figure 6 and the  $K_L$  data of Figure 7 depict the same trend as the wind speed increases.

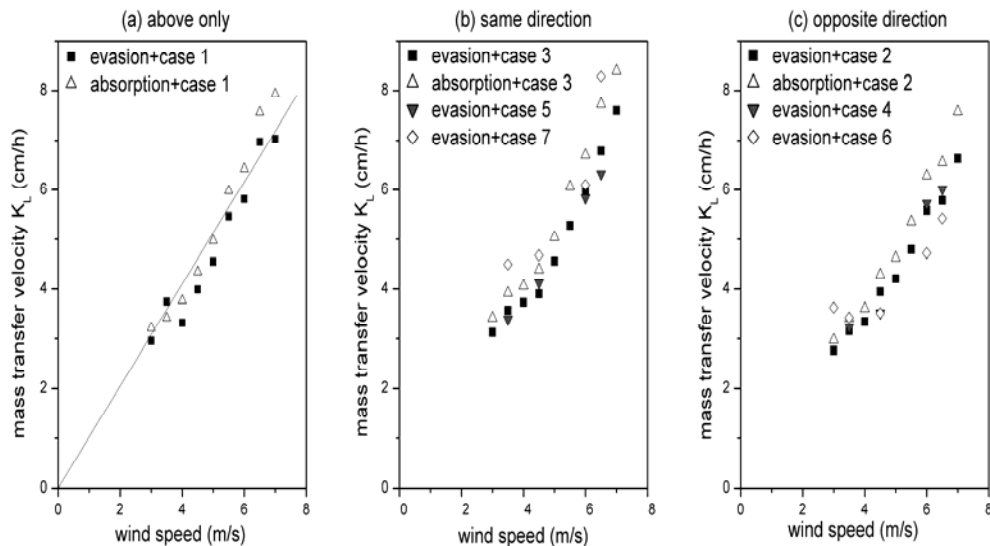


Figure 7: Mass transfer coefficient versus wind speed

For direct comparison with the previous results of Law & Khoo<sup>[1]</sup> and Jahne & Munnich<sup>[19]</sup> carried out in a similar circular wind-wave channel, the mass transfer coefficient is depicted together with  $Sc$  as  $K_L Sc^{0.5}$  for the ordinate axis and plotted

versus the wind speed on the abscissa axis. The use of  $K_L Sc^{0.5}$  assumes a relationship of  $K_L$  to the diffusion coefficient of the gas in water that has been employed by many others, and also to account for the different tracer gases utilized in the different experiments. It is noted that in Law & Khoo<sup>[1]</sup>, CO<sub>2</sub> was used at the water temperature of around 27°C ( $Sc \approx 420$ ). In Jahne & Munnich's work, CO<sub>2</sub> was used at the water temperature of around 20°C ( $Sc \approx 600$ ), while in this work, O<sub>2</sub> was used and employed at the water temperature was around 22°C ( $Sc \approx 532$ ). Figure 8 shows reasonably good concurrence in value and trend with Law & Khoo<sup>[1]</sup> and Jahne & Munnich<sup>[19]</sup>.

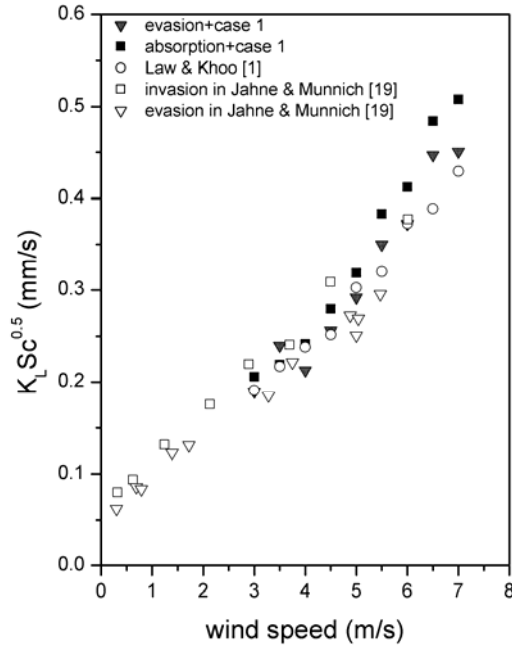


Figure 8: Comparison of the mass transfer coefficient varying with nominal wind speed

## Discussion

Correlation of the mass transfer coefficient and near surface turbulence parameters has been investigated by previous researchers, such as McCready et al<sup>[8]</sup>, Khoo & Sonin<sup>[20]</sup> and Tamburrino & Gulliver<sup>[6]</sup>. The relation can be expressed as:

$$K_L^+ \equiv \frac{K_L}{v_{\beta-rms}} = f \left( \left( \frac{\beta_{rms} v}{v_{\beta-rms}^2} \right)^{0.5} \right) Sc^{-0.5}. \quad (10)$$

Here  $K_L^+ \equiv K_L / v_{\beta-rms}$  is the non-dimensional mass transfer coefficient,

$\beta_{rms}^+ \equiv \frac{\beta_{rms} \nu}{v_{\beta-rms}^2}$  is the non-dimensional form of  $\beta_{rms}$ , and  $f( )$  indicates a functional

relationship. The exponent for Sc is governed by the surface conditions. McKenna & McGillis [4] investigated the role of surfactant in gas-water mass transfer and

presented an expression for the Schmidt number exponent as  $n = \frac{2}{3} - \frac{1}{6} e^{-\zeta/2}$

where  $\zeta$  is defined as stress ratio. In this work, mass transfer experiment is done in the condition of a clean surface. Under such conditions the stress ratio is zero, so the exponent of Sc is set to 0.5.

Figure 9 shows the plot of  $K_L^+ Sc^{0.5}$  versus  $(\beta_{rms}^+)^{0.5}$  for all the studied flow conditions based on both gas evasion and absorption measurements in our experiments. The result of Law & Khoo [1] is also included. In the work of Law & Khoo [1], turbulence is imposed through two distinct methods namely a wind-induced shear turbulence from above and separately a confined-jet turbulence induced from beneath in a half-filled cylinder with water. A wide range of various water-glycerol mixtures as the liquid and carbon dioxide gas were tested at different temperatures. A combination of their works where  $\beta_{rms}$  were explicitly measured with the present data will help to build a more universal correlation. It can be observed that a linear behavior (slope=0.20 with  $R^2=0.981$ ) can still be realized for all of the presented flow conditions. From Figure 9, a general relation can be proposed to correlate the mass transfer coefficient with the near surface turbulence parameters:

$$K_L^+ Sc^{0.5} = 0.2 (\beta_{rms}^+)^{0.5}. \quad (11)$$

A detailed comparison with other similar models can be found in Xu et al. [21]

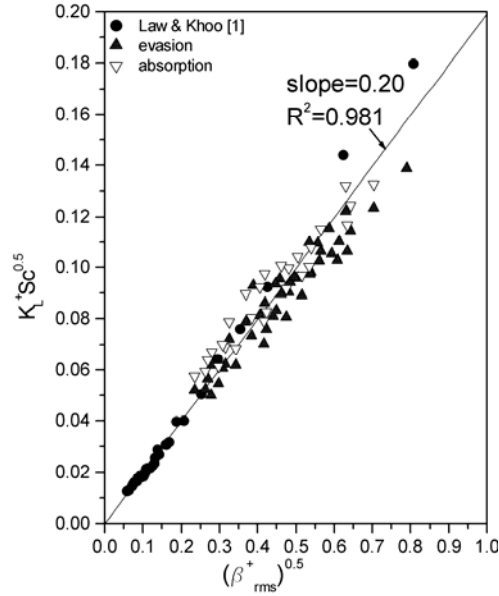


Figure 9:  $K_L^+ Sc^{0.5}$  versus  $(\beta_{rms}^+)^{0.5}$  for all the tested flow conditions

## Conclusion

It is increasingly clear that the employment of bulk turbulence is unable to provide a unique relationship between the turbulence hydrodynamics and the scalar transfer coefficient, and the flow hydrodynamics in the immediate vicinity of the interface like the vertical velocity gradient ( $\beta$  or the surface divergence) plays an important role in determining the transport process which is fairly independent of the means of turbulence generation. Based on the improved measurement method provided in this work, quantification of the vertical velocity with respect to the fluctuating interface and evaluation of the associated velocity gradient in the vicinity of the interface were carried out. The critical parameter  $\beta$  was obtained under vastly different and distinct flow conditions. These mentioned distinct flow conditions are turbulence induced by wind shear from above, turbulence generated and diffused to the free surface from beneath the interface, and a combination of contributing conditions from above and beneath the gas-liquid interface simultaneously. All of them can be regarded as the simplifications of all the other turbulence generation methods. Results from the mass transfer experiments suggests a possible general

relationship of the form,

$$\frac{K_L}{(\beta_{rms} \nu)^{0.5}} Sc^{0.5} = C \approx 0.20 \quad (19)$$

It can be found to correlate the interfacial hydrodynamics parameter and the mass transfer coefficient. The proposed correlation has found good concurrence at least in terms of trends with other reported works where turbulence is generated differently as in grid-stirred turbulence, a submerged moving bed plume, flow down an induced plane and others. The mentioned concurrence is true with  $C \sim O(1.0)$ .

## References:

- [1] Law CNS, Khoo BC. Transport across a Turbulent Gas-water Interface. *AICHE Journal*. 2002; 48: 1856-1868
- [2] Molder E, Tenno T, Mashirin A. The effect of surfactants on oxygen mass-transfer through the gas-water interface. *ESPR – Environ Sci & Pollut Res*, 2002; Special Issue 1: 39–42
- [3] Vasconcelos JMT, Rodrigues JML, Orvalho SCP, Alves SS, Mendes RL, Reis A. Effect of contaminants on mass transfer coefficients in bubble column and airlift contactors. *Chemical Eng Sci*. 2003; 58: 1431–1440
- [4] McKenna SP, McGillis WR. The role of free-surface turbulence and surfactants in gas-water gas transfer. *Int. J. Heat & Mass transfer*. 2004; 47: 539-553
- [5] Theofanous TG. Conceptual models of Gas Exchange. In: Brutsaert W, Jirka GH. *Gas transfer at water surfaces*. Dordrecht, Holland: D. Reidel Publishing company, 1984: 271-281
- [6] Tamburrino A, Gulliver JS. Free surface turbulence and mass transfer in a channel flow. *AICHE Journal*. 2002; 48: 2732-2743
- [7] Hanratty TJ. Effect of gas flow on physical adsorption. In: Wilhelm SC, Gulliver JS. *Air-water mass transfer*. New York: ASCE, 1991: 10-33
- [8] McCready MJ, Vassihadou E, Hanratty TJ. Computer simulation of turbulent mass transfer at a mobile interface. *AICHE Journal*. 1986; 32: 1108-1115

- [9] Hassan YA, Okamoto K, Philip OG. Investigation of the interaction between a fluid flow and the fluid's free surface using particle image velocimetry. In the Ninth International Symposium on Transport Phenomena in Thermal-Fluids Engineering (ISTP-9). Singapore, 1996: 566-574
- [10] Peirson WL. Measurement of surface velocities and shears at a wavy gas-water interface using particle image velocimetry. *Experiments in Fluids*. 1997; 23: 427-437
- [11] Law CNS, Khoo BC, Chew TC. Turbulence structure in the immediate vicinity of the shear-free air-water interface induced by a deeply submerged jet. *Experiments in Fluids*. 1999; 27: 321-331
- [12] Jahne B, Wierzimok D. Measurement of wave-induced turbulent flow structures using digital image sequence analysis. In: Wilhelm SC, Gulliver JS. *Air-water mass transfer*. New York: ASCE, 1991: 200-209
- [13] Lorencez C, Nasr-Esfahany M, Kawaji M. Turbulence structure and prediction of interfacial heat and mass transfer in wavy-stratified flow. *AICHE Journal*. 1997; 43: 1426-1435
- [14] Baumann KH, Muhlfridel K. Mass transfer and concentration profiles near phase boundaries. *Int. J. Therm. Sci.* 2001; 40: 425-436
- [15] Lin HJ, Perlin M. Improved methods for thin surface boundary layer investigations. *Experiments in Fluids*. 1998; 25: 431-444
- [16] Munsterer T, Jahne B. LIF measurements of concentration profiles in the aqueous mass boundary layer. *Experiments in Fluids*. 1998; 25: 190-196
- [17] Ridler TW, Calvard S. Picture thresholding using an iterative selection method. *IEEE Trans Syst Man Cybern* 1978; 8: 630-632
- [18] Katznelson R. DQM standard operation procedure (SOP) 9.2.1.2(V3). 2004; <http://www.swrcb.ca.gov/nps/docs/cwtguidance/9212sop.pdf>
- [19] Jahne B, Munnich KO. Measurements of gas exchange and momentum transfer in a circular wind-wave tunnel. *Tellus*. 1979; 31: 321-329
- [20] Khoo BC, Sonin AA. Scalar rate correlation at a turbulent water free surface: a two-regime correlation for high Schmidt number. *Int. J. Heat Mass Transfer*. 1992; 35: 2233-2244
- [21] Xu ZF, Khoo BC, Carpenter K. Mass transfer across the turbulent gas-water interface. *AICHE Journal*, In press